

# CCD Washington photometry of four poorly studied open clusters in the two inner quadrants of the galactic plane

N. Marcionni<sup>a,\*</sup>, J. J. Clariá<sup>a,b,1</sup>, M. C. Parisi<sup>a,b</sup>, T. Palma<sup>a,b,1</sup>, M. Oddone<sup>a</sup>,  
A. V. Ahumada<sup>a,b,1</sup>

<sup>a</sup>*Observatorio Astronómico, Universidad Nacional de Córdoba, Laprida 854, Córdoba, Argentina*

<sup>b</sup>*Consejo Nacional de Investigaciones Científicas y Técnicas, CONICET, Argentina*

---

## Abstract

Complementing our Washington photometric studies on Galactic open clusters (OCs), we now focus on four poorly studied OCs located in the first and fourth Galactic quadrants, namely BH 84, NGC 5381, BH 211 and Czernik 37. We have obtained CCD photometry in the Washington system  $C$  and  $T_1$  passbands down to  $T_1 \sim 18.5$  magnitudes for these four clusters. Their positions and sizes were determined using the stellar density radial profiles. We derived reddening, distance, age and metallicity of the clusters from extracted  $(C - T_1, T_1)$  color-magnitude diagrams (CMDs), using theoretical isochrones computed for the Washington system. There are no previous photometric data in the optical band for BH 84, NGC 5381 and BH 211. The CMDs of the observed clusters show relatively well defined main sequences, except for Czernik 37, wherein significant differential reddening seems to be present. The red giant clump is clearly seen only in BH 211. For this cluster, we estimated the age in  $(1000^{+260}_{-200})$  Myr, assuming a metallicity of  $Z = 0.019$ . BH 84 was found to be much older than it was previously believed, while NGC 5381 happened to be much younger than previously reported. The heliocentric distances to these clusters are found to range between 1.4 and 3.4

---

\*Corresponding author

*Email addresses:* [nahuel@oac.uncor.edu](mailto:nahuel@oac.uncor.edu) (N. Marcionni), [claria@oac.uncor.edu](mailto:claria@oac.uncor.edu) (J. J. Clariá), [celeste@oac.uncor.edu](mailto:celeste@oac.uncor.edu) (M. C. Parisi), [tali@oac.uncor.edu](mailto:tali@oac.uncor.edu) (T. Palma), [mao@oac.uncor.edu](mailto:mao@oac.uncor.edu) (M. Oddone), [andrea@oac.uncor.edu](mailto:andrea@oac.uncor.edu) (A. V. Ahumada)

<sup>1</sup>Visiting Astronomer, CTIO.

kpc. BH 84 appears to be located at the solar galactocentric distance, while NGC 5381, BH 211 and Czernik 37 are situated inside the solar ring.

*Keywords:* Galaxy: open clusters and associations: individual: BH 84, NGC 5381, BH 211, Czernik 37 - Techniques: photometric

---

## 1. Introduction

Galactic open clusters (OCs) have long been considered excellent targets not only to probe the Galactic disc properties (Lyngå, 1982; Friel, 1995; Piskunov et al., 2006; Bica et al., 2006) but also to trace its chemical evolution (see, e.g., Chen et al., 2003 and references therein). Because it is relatively simple to estimate ages, distances and metallicities of OCs fairly accurately, their basic parameters constitute excellent tracers to the structure and chemical evolution of the Galactic disc. The proximity of most OCs to the Galactic plane, however, usually restricts this analysis to the most populous ones and/or to those located within a few kpc from the Sun (Bonatto et al., 2006). Although there are at present estimates of a total of about  $25 \times 10^3$  OCs in the Milky Way (Portegies Zwart et al., 2010), there is not yet an estimation of fundamental parameters such as reddening, distance and age for nearly 30% of the  $\sim 2200$  catalogued Galactic OCs (Dias et al., 2002; Bica et al., 2003; Dutra et al., 2003).

The present work is part of a current project of photometric observation of Galactic OCs in the Washington system that is being developed at the Observatorio Astronómico de la Universidad Nacional de Córdoba (Argentina). This project aims at determining the fundamental parameters or at refining the quality of observationally determined properties for some unstudied or poorly studied OCs, located in different regions of the Milky Way. Washington photometry has proved to be a valuable tool to determine the fundamental parameters of OCs since information on cluster membership, reddening, distance, age and metallicity is obtained through the analysis of the  $(C - T_1, T_1)$  color-magnitude diagram (CMD). We have already reported results based on Washington CCD  $CT_1$  photometric data on several young (e.g., Piatti et al. 2003a), intermediate-age (e.g., Clariá et al., 2007) and old Galactic OCs (e.g., Piatti et al. 2004). These studies have contributed not only to the individual characterization of these stellar systems but also to the global understanding of some properties of the Galactic disc (e.g., Parisi et al. 2005).

In this study we provide new high-quality photometric CCD data obtained with the Washington system  $C$  and  $T_1$  passbands down to  $T_1 \sim 18.5$  magnitudes in the fields of four faint, poorly studied OCs, namely BH 84, NGC 5381, BH 211 and Czernik 37. The equatorial and Galactic coordinates of the cluster centers taken from the WEBDA Open Cluster Database (Mermilliod, 2005) are listed in Table 1, together with the angular sizes given by Archinal & Hynes (2003). The selected clusters are located in the first and fourth Galactic quadrants ( $280^\circ < l < 3^\circ$ ) near the Galactic plane ( $|b| \leq 3^\circ$ ). As far as we know, no previous photometric data in the optical band exist for BH 84, NGC 5381 and BH 211. The four selected clusters have been examined by Bukowiecki et al. (2011) and Tadross (2008, 2011) using Two-Micron All-Sky Survey (2MASS) data. Some preliminary results about BH 84, NGC 5381 and BH 211 are presented in Marcionni et al. (2013). A brief description of these objects as well as a summary of previous results for the fields under investigation is given below:

*BH 84.* First recognized as an OC by van den Bergh & Hagen (1975), this object (IAU designation C0959-579) seems to be a detached, relatively poor and faint OC in the Carina constellation (Fig. 1). It shows the typical morphology of a Trumpler class II-1p cluster, which is characterized by a slight concentration of member stars of similar brightness and relatively small population. The only observational data for this object are those given in the 2MASS catalog and discussed by Bukowiecki et al. (2011). These authors derived a reddening  $E(B - V) = 0.60$  and suggest that BH 84 is a young cluster ( $\sim 18$  Myr), located at a heliocentric distance  $d = (2.92 \pm 0.19)$  kpc.

*NGC 5381.* This is a cluster in Centaurus, also designated as BH 156 (van den Bergh & Hagen, 1975). Archinal & Hynes (2003) refer to this object as belonging to Trumpler class II-2m, i.e., a moderately rich, detached cluster with little central concentration and medium-range bright stars (Fig. 1). According to these authors, NGC 5381 has a comparatively large angular diameter of  $11'$ . A search for variable stars in the cluster field was carried out by Pietrzyński et al. (1997). Using 2MASS data, Tadross (2011) suggests that NGC 5381, slightly reddened by  $E(B - V) = 0.06$ , is an intermediate-age cluster ( $\sim 1.6$  Gyr) located at 1.2 kpc from the Sun.

*BH 211.* This object (C1658-410) appears to be somewhat elongated in the East-West direction (Fig. 1). BH 211 is a detached, moderately poor and relatively faint group of stars, first recognized as an OC in Scorpius by van den Bergh & Hagen (1975). It is a small-sized OC situated very near the

Galactic center direction, practically on the Galactic plane (Table 1). The only observational data-set for this object is the one given in the 2MASS catalog and discussed by Bukowiecki et al. (2011) who found the following results:  $E(B - V) = 0.48$ ,  $d = (1.38 \pm 0.09)$  kpc and  $\sim 1.6$  Gyr.

*Czernik 37*. Also known as BH 253 (van den Bergh & Hagen, 1975), this is a relatively faint cluster (C1750-273) first recognized in Sagittarius by Czernik (1966). As indicated by its Trumpler class (II-1m), it shows a slight central concentration but can be identified by its relatively dense population compared to that of the field stars (Fig. 1). This cluster is projected on to the central bulge of the Galaxy, only  $2^\circ$  from the Galactic center direction. Carraro et al. (2005) presented CCD *BVI* photometry in the field of Czernik 37. Although they conclude that this may be a sparse but real cluster superimposed on the Galactic bulge population, they do not provide its physical parameters. Using 2MASS data, Tadross (2008) derived a heliocentric distance of 1.7 kpc,  $E(B - V) = 1.03$  and an age of 0.6 Gyr.

The layout of this paper is as follows. Section 2 provides details on our observations and the data reduction procedure. In Section 3 we determine the cluster centers and the stellar density radial profiles. Section 4 deals with the determination of cluster fundamental parameters through the fitting of theoretical isochrones. A brief description of the results, including a comparison with previous findings, is presented in Section 5, while the final conclusions are summarized in Section 6.

## 2. Observations and reductions

The observations of the selected clusters were carried out with the Cerro Tololo Inter-American Observatory (CTIO, Chile) 0.9 m telescope, during the nights of 2008 May 9-11, with a  $2048 \times 2048$  pixel Tektronix CCD. The scale on the chip is  $0.396'' \text{ pixel}^{-1}$  (focal ratio  $f/13.5$ ) yielding a visual field of  $13.6' \times 13.6'$ . We controlled the CCD through the CTIO ARCON 3.3 data acquisition system in the standard quad amplifier mode, with a mean gain and readout noise of  $1.5 \text{ e}^-/\text{ADU}$  and  $4.2 \text{ e}^-$ , respectively. The filters used were the Washington system *C* (Canterna, 1976) and Kron-Cousins  $R_{KC}$ . The latter has a significantly higher through-put as compared with the standard Washington  $T_1$  filter but  $R_{KC}$  magnitudes can be accurately transformed to yield  $T_1$  magnitudes (Geisler, 1996). From here onwards, we will use indistinctly the words  $R_{KC}$  or  $T_1$ . Typically 20 standard stars taken from the list of Geisler (1996), covering a wide range in color, were nightly observed.

Table 2 shows the log of the observations with dates, filters, exposure times and airmasses. In addition, a series of 10 bias and five dome and sky flat-field exposures per filter were obtained nightly. The weather conditions kept very stable at CTIO, with a typical seeing of 1.0''-1.2'', although some images have slightly larger full-widths at half maximum (FWHMs) due to temperature changes of up to 2 °C. Fig. 1 shows schematic finding charts of the observed cluster fields built with all the measured stars in the  $T_1$  band.

The  $CT_1$  images were reduced at the Observatorio Astronómico de la Universidad Nacional de Córdoba (Argentina) with IRAF<sup>2</sup>, using the QUADPROC package. After applying the overscan-bias subtraction for the four amplifiers independently, we carried out flat-field corrections using a combined sky-flat frame, which was previously checked for nonuniform illumination pattern with the averaged dome-flat frame. Then, we did aperture photometry for the standard star fields using the PHOT task within DAOPHOT II (Stetson, 1991). The relationships between instrumental and standard magnitudes were obtained by fitting the equations:

$$c = a_1 + T_1 + (C - T_1) + a_2 \times X_C + a_3 \times (C - T_1), \quad (1)$$

$$r = b_1 + T_1 + b_2 \times X_{T_1} + b_3 \times (C - T_1), \quad (2)$$

where  $X$  represents the effective airmass and capital and lowercase letters stand for standard and instrumental magnitudes, respectively. The coefficients  $a_i$  and  $b_i$  ( $i = 1, 2$  and  $3$ ) were nightly derived through the IRAF routine FITPARAM. The resulting mean coefficients together with their errors are shown in Table 3; the typical rms errors of equations (1) and (2) are 0.017 and 0.015 mag, respectively, indicating the nights were of good photometric quality.

Point spread function (PSF) photometry for the selected fields was performed using the stand-alone version of the DAOPHOT II package (Stetson, 1994), which provided us with  $x$  and  $y$  coordinates and instrumental  $c$  and  $r$  magnitudes for all the stars identified in each field. The PSFs were generated from two samples of 35-40 and  $\sim 100$  stars interactively selected. For each frame, a quadratically varying PSF was derived by fitting the stars in the

---

<sup>2</sup>IRAF is distributed by the National Optical Astronomy Observatories, which is operated by the Association of Universities for Research in Astronomy, Inc., under contract with the National Science Foundation

larger sample, once their neighbors were eliminated using a preliminary PSF obtained from the smaller star sample, which contained the brightest, least contaminated stars. We then used ALLSTAR program to apply the resulting PSF to the identified stellar objects and create a subtracted image, which was used to find and measure magnitudes of additional fainter stars. The PSF magnitudes were determined using as zero points the aperture magnitudes yielded by PHOT. This procedure was repeated three times on each frame. Next, we computed aperture corrections from the comparison of PSF and aperture magnitudes using the subtracted neighbor PSF star sample. The resulting aperture corrections were on average less than 0.02 mag (absolute value) for  $c$  and  $r$ , respectively. Note that PSF stars are distributed throughout the whole CCD frame, so that variations of aperture corrections should be negligible. Finally, the standard magnitudes and colors for all the measured stars were computed by inverting equations (1) and (2), once positions and instrumental  $c$  and  $r$  magnitudes of stars in the same field were matched using Stetson's DAOMATCH and DAOMASTER programs.

Once we obtained the standard magnitudes and colors, we built a master table containing the average of  $T_1$  and  $C - T_1$ , their errors  $\sigma(T_1)$  and  $\sigma(C - T_1)$  and the number of observations for each star, respectively. We derived magnitudes and colors for 1884, 2439, 979 and 1129 stars in the fields of BH 84, NGC 5381, BH 211 and Czernik 37, respectively. These values are provided in Tables 4-7. Magnitude and color errors are the standard deviation of the mean or the observed photometric errors for stars with only one measurement. Tables 4-7 are only partially presented here as guidance, regarding their form and content. The complete tables can be found on the on-line version of the journal.

Fig. 2 shows the behavior of the  $T_1$  and  $C - T_1$  photometric errors as a function of  $T_1$  for stars measured in the field of NGC 5381, the most populated observed field. Note that  $\sigma T_1$  and  $\sigma(C - T_1)$  appear to be smaller than 0.04 magnitudes for stars brighter than  $T_1 \sim 18.5$  and 17.5 magnitudes, respectively. The bright stars having large associated errors are stars saturated in all frames, bits of stars or even failures in the detector erroneously taken as stars by DAOPHOT. It can be observed in Section 4 that these stars do not affect at all the fundamental parameter determination of the observed clusters. Bearing in mind the behavior of the photometric errors with the  $T_1$  magnitude for the observed stars in Fig. 2, we trust the accuracy of the morphology and position of the main cluster features in the  $(C - T_1, T_1)$  CMDs. Fig. 3 shows these CMDs for all the observed stars in the different fields.

They appear to be contaminated by field stars, as should be expected since all the studied OCs are projected on to the Galactic center direction. As can be seen in Fig 3, the faintest  $T_1$  magnitudes obtained for each cluster are such that they allow the mapping of most of the cluster main sequences (MSs). If there are still fainter stars in the clusters, then they practically do not add any information to the one already obtained. Cluster MSs appear as broad sequences of stars among crowded field features. On the other hand, a group of comparatively bright late-type stars in BH 211 seems to form the cluster red giant clump (RGC) centered at  $T_1 \sim 12.5$  and  $(C - T_1) \sim 3.2$  magnitudes, which indicates that we are possibly dealing with an intermediate-age OC.

### 3. Determining the center and size of the clusters

To determine the central position of the clusters on a firm basis, we applied a statistical method consisting in tracing the stellar density profiles projected on to the directions of the  $x$  and  $y$ -axes. The coordinates of the clusters' centers and their estimated uncertainties were determined by fitting Gaussian distributions to the star counts in the  $x$  and  $y$  directions for each cluster. The fits of the Gaussians were performed using the NGAUSSFIT routine in the STSDAS/IRAF package. We adopted a single Gaussian and decided to fix the constant and the linear terms to the corresponding background levels and to zero, respectively. We used as variables the center of the Gaussian, its amplitude and its FWHM. After eliminating a couple of scattered points, the fitting procedure converged after one iteration on average. The stars projected along the  $x$  and  $y$  directions were counted within intervals of 50 pixels in BH 84 and NGC 5381 and within intervals of 75 pixels in BH 211 and Czernik 37. We determined the central position of the clusters with a typical NGAUSSFIT standard deviation of  $\pm 10$  pixels ( $\sim 4''$ ) in all cases. The centers of the Gaussians were finally fixed at  $(X_C, Y_C) = (969, 1040)$ ,  $(940, 1012)$ ,  $(964, 1145)$  and  $(894, 1105)$  pixels for BH 84, NGC 5381, BH 211 and Czernik 37, respectively. These values were adopted for the analysis that follows. Cluster centers are marked by a cross in Fig. 1.

We then built clusters' radial profiles, from which we estimated the cluster radii, generally used as an indicator of cluster dimensions. Cluster stellar density radial profiles are usually built by counting the number of stars distributed in concentric rings around the cluster center and normalizing the sum of stars in each ring to the unit area. Although this procedure allows us to stretch the radial profile to its utmost, until complete circles can no

longer be traced in the observed field, we preferred to follow another method in order to move even further away from the cluster center. This method is based on counts of stars located in boxes of 50 pixels a side, distributed throughout the whole field of each cluster. Thus, the number of stars per unit area at a given  $r$  can be directly calculated through the expression:

$$(n_{r+25} - n_{r-25}) / [(m_{r+25} - m_{r-25}) \times 50^2], \quad (3)$$

where  $n_j$  and  $m_j$  represent the number of counted stars and boxes included in a circle of radius  $j$ , respectively. Note that this procedure does not necessarily require a complete circle of radius  $r$  within the observed field to estimate the mean stellar density at such distance. It is important to consider this fact since having a stellar density profile which extends far away from the cluster center allows us to estimate the background level with higher precision. This is necessary to derive the cluster radius ( $r_{cl}$ ), defined as the distance from the cluster center where the stellar density profile intersects the background level. It is also helpful to measure the FWHM of the stellar density profile, which plays an important role in the construction of the cluster CMDs. The resulting density profiles expressed as number of stars per unit area in arcmin<sup>2</sup> are presented in Fig. 4. The uncertainties estimated at various distances from the cluster centers follow Poisson statistics. The new equatorial coordinates derived for the clusters in this study are listed in Table 1, while columns 2-4 of Table 8 list the radii at the FWHM ( $r_{FWHM}$ ), the estimated radii which yield the best enhanced cluster fiducial features ( $r_{clean}$ ) and the cluster radii ( $r_{cl}$ ). The different linear radii in parsecs were determined using the heliocentric distances derived in Section 4.

#### 4. Cluster fundamental parameter estimates

CMDs covering different circular extractions around each cluster center were constructed, as shown in Figs. 5-8. The panels in the figures are arranged, from left to right and from top to bottom, in such a way that they exhibit the variations in stellar population from the innermost to the outermost regions of the cluster fields. We started with the CMD for stars distributed within  $r < r_{FWHM}$ , followed by those of the cluster regions delimited by  $r < r_{clean}$  and  $r < r_{cl}$  and finally by the adopted field CMD. We used the CMDs corresponding to the stars within  $r_{FWHM}$  as the cluster fiducial sequence references. Then, we varied the distance from the cluster centers, starting at



$r_{FWHM}$ . Next, we built different series of extracted CMDs. Finally, we chose those CMDs - one per cluster - which maximize the star cluster population and minimize the field star contamination in the CMDs. The main cluster features can be identified by inspecting the right top panels of Figs. 5-8. Note that the cluster MSs look well populated, particularly in NGC 5381, all of them showing clear evidence of evolution. These MSs develop along  $\sim 5$  magnitudes in BH 84 and Czernik 37 and along  $\sim 5-6$  magnitudes in NGC 5381 and BH 211. The hook at the MS turnoff of BH 211's CMD and the RGC centered at  $T_1 \sim 12.5$  and  $C - T_1 \sim 3.2$  magnitudes indicate that we are dealing with an intermediate-age OC. The width of the clusters' MSs is clearly not the result of photometric errors, since these hardly reach a tenth of magnitude at any  $T_1$  level. Thus, such width could be caused by intrinsic effects (binarity, rotation, evolution, etc.), by differential reddening and/or by field star contamination. To derive the cluster fundamental parameters, we will use the CMDs with  $r < r_{clean}$ .

Although, as we mentioned above, the broadness of the clusters' MSs is certainly due to several effects, in the particular case of Czernik 37, a clear variation of the interstellar reddening across the cluster field seems to be present. In case this effect indeed existed in the remaining clusters, it is by far less evident. The lower limit estimated by Burki (1975) for clusters with differential reddening is  $\Delta(B - V) = 0.11$ , which corresponds to  $\Delta(C - T_1) = 0.22$ , if a value of 1.97 for the  $E(C - T_1)/E(B - V)$  ratio (Geisler, 1996) is adopted. From the right top panel of Fig. 8, we estimated  $\Delta(C - T_1) \sim 1.0$  mag for Czernik 37, a value which largely exceeds the limit established by Burki (1975). The existence of differential reddening in Czernik 37 makes the determination of its fundamental parameters very difficult, particularly its reddening and its heliocentric distance. It is for this reason that the resulting parameters for Czernik 37 present associated errors larger than in the other clusters.

The widely used procedure of fitting theoretical isochrones to observed CMDs was employed to estimate the  $E(C - T_1)$  color excess, the  $T_1$ - $M_{T_1}$  apparent distance modulus and the age and metallicity of the clusters. It is well known that the metallicity of a cluster plays an important role when its age is estimated from the fit of theoretical isochrones. Indeed, isochrones with the same age but with different metallicities can range from slightly to remarkably distinguishable, depending on their sensitivity to metal content. The  $(C - T_1, T_1)$  CMD, for example, is nearly three times more metal sensitive than the  $(V - I, V)$  CMD (Geisler & Sarajedini, 1999). The distinction is

particularly evident for the evolved phases of the RGC and the giant branch. As far as zero-age main sequences (ZAMSs) are concerned, they are often less affected by metallicity effects, and can even exhibit imperceptible variations for a specific metallicity range within the photometric errors. This is the case of Galactic OCs, therefore including the four clusters here studied. Since there are no previous available estimates of their metallicities, we followed the general rule of starting by the adoption of both solar ( $Z = 0.019$ ) and sub-solar ( $Z = 0.008$ ) values for the clusters' metal content.

As for the isochrone sets, we used those computed by the Padova group (Girardi et al., 2002) in steps of  $\Delta \log \text{age} = 0.05$  dex. As shown in previous studies (e.g., Piatti et al., 2003b), these isochrones lead to results similar to those derived from the Geneva group's isochrones (Lejeune & Schaerer, 2001). We preferred to use the Padova group's isochrones because they reach fainter magnitudes, thus allowing a better fit to the cluster fainter portions of the MSs. Then, we first selected ZAMSs with  $Z = 0.019$  and  $0.008$  ( $[\text{Fe}/\text{H}] = 0.0$  and  $-0.4$  dex) and fitted these ZAMSs to the cluster CMDs to derive color excesses and apparent distance moduli for each selected metallicity. Since the fits are performed through the lower envelope of the cluster's MSs, the presence of binaries practically does not affect the choice of the best isochrones. Note that when  $Z = 0.019$  is used in the fits, the resulting cluster reddenings and distances turn out to be slightly larger than the values obtained using  $Z = 0.008$ . The increases in distance vary from 250 pc to 500 pc depending on the cluster, while the increase in reddening is within error limits. Then, using each of the derived  $[E(C - T_1), T_1 - M_{T_1}]_Z$  sets, we performed isochrone fits. We repeated the fits for a larger number of isochrones covering appropriate age ranges according to each cluster. The brightest magnitude in the MS, the bluest point of the turnoff and the locus of the RGC, when visible, were used as reference points during the fits. Finally, we chose the best fit for each  $[E(C - T_1), T_1 - M_{T_1}]_Z$  set and compared all the individual best fits to choose the one which best reproduced the cluster features. In all cases, the best fits were done only by eye and they were obtained using solar metallicity isochrones. We would like to point out that the bright stars with very large associated errors in Fig. 2 correspond to objects located beyond NGC 5381  $r_{\text{clean}}$ . For this reason, these stars do not affect the cluster parameter determination in NGC 5381. Something similar occurs with the other three studied clusters.

Fig. 9 illustrates the results of our task, while Table 9 lists the estimated  $E(B - V)$  color excesses, heliocentric distances, ages and metallicities of

the clusters. Their errors were derived taking into account the broadness of the cluster MSs and, in the case of the cluster distances, the expression  $0.46 \times [\sigma(V - M_V) + 3.2 \times \sigma E(B - V)] \times d$ , where  $\sigma(V - M_V)$  and  $\sigma(E(B - V))$  represent the estimated errors in  $V - M_V$  and  $E(B - V)$ , respectively (see, e.g., Clariá et al., 2007). The expressions  $E(C - T_1) = 1.97 \times E(B - V)$  and  $M_{T_1} = T_1 + 0.58 \times E(B - V) - (V - M_V)$  taken from Geisler (1996) were used to relate both color excesses and distance moduli. We also list in Table 9 the Galactocentric rectangular coordinates  $X, Y, Z$  and the Galactocentric distances  $R_{GC}$  of the clusters, derived assuming the Sun’s distance from the center of the Galaxy to be 8.5 kpc. The adopted reference system is centered on the Sun, with the  $X$  and  $Y$ -axes lying on the Galactic plane and  $Z$  perpendicular to the plane.  $X$  points towards the Galactic center, being positive in the first and fourth quadrants;  $Y$  points in the direction of the Galactic rotation, being positive in the first and second Galactic quadrants.  $Z$  is positive towards the north Galactic pole.

## 5. Results

The 2MASS catalog has been widely used to determine the fundamental parameters of hundreds of OCs (see, e.g., Kronberger et al., 2006; Bonatto & Bica 2007; Tadross 2011). The results obtained, however, do not always yield consistent results with those derived using optical data. As shown by Dias et al. (2012), the accuracy in determining the color excess  $E(J - H)$  using only 2MASS is mainly limited by structural uncertainty in the MS and/or narrow range of magnitude sampling of the MS. From the observational point of view, the main reason for this discrepancy is the limiting magnitude, particularly for the oldest clusters, which reflects in the sampling of the MS, together with photometric errors. Note that 2MASS photometric errors typically reach 0.10 magnitudes at  $J \leq 16.2$  and  $H \leq 15.0$  (Soares & Bica, 2002), while in the optical bands ( $UBV$  or  $CT_1$ , for example), they are typically lower than 0.05 magnitudes at  $V \leq 18.0$  and  $T_1 \leq 19.0$ . In the following subsections, we compare the current results with those obtained in previous studies using 2MASS.

### 5.1. BH 84

The equatorial coordinates we derived for the center of BH 84 differ only by  $33''$  in declination from the WEBDA value (Table 1). The radial number density profile of BH 84 is shown in Fig.4, from which we derive a radius of

3.6', slightly lower than the value reported by Archinal & Hynes (2003). The cluster MS is easily identifiable in Fig. 5, extending along  $\sim 5$  magnitudes and with clear evidence of some evolution. Outer Galactic disc stars remarkably contaminate the cluster MS, particularly its fainter half portion. The solar metallicity ZAMS fitted to the cluster CMD yields a reddening  $E(C - T_1) = 1.25 \pm 0.10$ , equivalent to  $E(B - V) = 0.63 \pm 0.05$ , and a true distance modulus  $(T_1)_o - M_{T_1} = 12.64 \pm 0.15$ , which implies a distance of  $(3.37 \pm 0.48)$  kpc from the Sun. For  $Z = 0.019$ , the best-fitting isochrone corresponds to an age of  $(560^{+150}_{-110})$  Myr (Fig. 9). Therefore, BH 84, situated at 142 pc below the Galactic plane and  $\sim 8.58$  kpc from the Galactic center (Table 9), is found to be a cluster only slightly younger than the Hyades. Both the reddening and the distance here derived show a reasonable agreement with the results from 2MASS data (Bukowiecki et al., 2011). Surprisingly, however, the age we find is significantly larger than Bukowiecki et al. (2011) estimate of 18 Myr. Although some of the 2MASS error must be due to the larger pixels, we believe the authors' gross underestimation of BH 84 age is clearly the result of the impossibility to see the turnoff point in the  $(J - K, J)$  diagram. Hence, Bukowiecki et al. (2011) derived the cluster's age just by fitting the ZAMS.

## 5.2. NGC 5381

This appears to be a large cluster covering nearly the entire observed field (Fig.1). We derived for NGC 5381 practically the same equatorial coordinates as those listed in WEBDA (Table 1). It is difficult, however, to estimate the cluster radius from the stellar density radial profile (Fig. 4), because it does not present a typical cluster-like structure. If the area for  $r > 1200$  pixels is considered to be the "star field area", then NGC 5381 seems to have a relatively small but conspicuous nucleus and a low-density extended corona (see also Fig. 1). We estimate the angular core and corona radii as  $\sim 330$  pixels ( $\sim 2.2'$ ) and 870 pixels ( $\sim 5.7'$ ), respectively. Fig. 3 reveals a crowded broad sequence of stars that traces the cluster MS along  $\sim 5$ -6 magnitudes and with clear signs of evolution. This fact suggests that the age of the cluster is some hundred million years. A number of stars visible in Fig. 9 with  $T_1$  magnitudes between 18 and 19 and  $(C - T_1)$  colors ranging from 0.5 up to 1.5 magnitudes are clearly background stars. No clump of red stars is visible. However, the analysis of 2MASS data by Tadross (2011) reveals that NGC 5381 is an intermediate-age (1.6 Gyr) cluster, suffering low interstellar extinction. This is not confirmed by the current optical data.

In fact, our best fit of the solar metallicity ZAMS in the  $(C - T_1, T_1)$  CMD yields  $E(C - T_1) = 0.90 \pm 0.08$ , equivalent to  $E(B - V) = 0.46 \pm 0.04$ , and a heliocentric distance of  $(2.63 \pm 0.40)$  kpc, while an age of about  $(250^{+65}_{-50})$  Myr is derived from the best-fitting isochrone (Fig. 9). Therefore, NGC 5381 now appears to be significantly younger than previously believed. The age difference between ours and Tadross (2011) may depend at least partially on the reddening difference. Our reddening estimate,  $E(B - V) = 0.46$ , is quite larger than the value of  $E(B - V) = 0.06$  reported by Tadross (2011). Therefore, a smaller age value is obtained when a larger reddening value is adopted. NGC 5381 lies at  $\sim 100$  pc above the Galactic plane and  $\sim 7.04$  kpc from the Galactic center (Table 9).

### 5.3. BH 211

The coordinates for the cluster center derived in the current study differ by  $\sim 15''$  in right ascension and by only  $3''$  in declination from the WEBDA values (Table 1). From the stellar density radial profile (Fig. 4), we determined the radius of BH 211 to be  $\sim 3.9'$ , in very good agreement with the value reported by Archinal & Hynes (2003). The  $(C - T_1, T_1)$  CMD obtained using all the measured stars in the cluster field is depicted in Fig. 3, wherein the main cluster features can be identified. What first calls our attention is the cluster MS, which looks well populated, has clear signs of evolution and develops along  $\sim 5$ -6 magnitudes. It is relatively broad, especially in its lower envelope, partly due to field star contamination. Another interesting feature of the  $(C - T_1, T_1)$  CMD is the presence of a number of good candidates for giant clump stars centered at  $(C - T_1, T_1) = (3.2, 12.5)$ . Since these stars lie within 400 pixels ( $2.6'$ ) from the cluster center, we may reasonably expect many of them to be cluster giants. The reddening and age we find,  $E(B - V) = 0.61 \pm 0.05$  and  $\sim (1000^{+260}_{-200})$  Myr (Table 9), turn out to be somewhat larger and lower, respectively, than Bukowiecki et al. (2011) estimates. In any case, there seems to be no doubt that BH 211 is an intermediate-age cluster located at about  $(1.44 \pm 0.21)$  kpc from the Sun, at scarcely  $\sim 12$  pc out of the Galactic plane and  $\sim 7.12$  kpc from the Galactic center (Table 8).

### 5.4. Czernik 37

The equatorial coordinates we derived for this cluster are different by  $15''$  in right ascension and by  $36''$  in declination (Table 1) from the WEBDA values. The radial number density profile of Czernik 37 is shown in Fig. 4, from which we derived a radius of  $3.6'$ , in good agreement with the value

reported by Archinal & Hynes (2003). This cluster appears to be embedded in the dense stellar population towards the Galactic bulge so that their properties are difficult to be determined. Although the cluster CMD (Fig. 3) is profusely contaminated by field stars, there is an appearance of a broad MS with evidence of some evolution. As mentioned in Section 4, the broadness of the MS of Czernik 37 is caused not only by field star contamination and other effects (binarity, rotation, photometric errors, etc.) but also by differential reddening. Such effect is probably due to the presence of irregularly distributed dark clouds, projected towards the cluster. Different isochrone fittings using  $Z = 0.019$  in Fig. 9 allow us to estimate the variation range of  $E(C - T_1)$  as  $\sim 1.0$  mag. The solar metallicity ZAMS which best fits the cluster CMD (Fig. 9) yields a reddening  $E(C - T_1) = 2.90 \pm 0.50$ , equivalent to  $E(B - V) = 1.47 \pm 0.25$ , and a true distance modulus  $(T_1)_o - M_{T_1} = 10.80 \pm 0.50$ . The isochrone corresponding to an age of  $(250^{+100}_{-65})$  Myr reasonably reproduces the main cluster features in Fig. 9. These results place Czernik 37 at a distance of  $(1.44 \pm 0.86)$  kpc from the Sun and  $\sim 7.1$  kpc from the Galactic center (Table 9). The current cluster parameters exhibit a rather poor agreement with those derived by Tadross (2008) from 2MASS data. As in NGC 5381, our larger  $E(B-V)$  value compared to that of Tadross (2008) may partly explain our lower age estimate.

## 6. Conclusions

We have presented new CCD Washington  $CT_1$  photometry in the field of four Galactic OCs projected onto the two inner quadrants of the Galactic plane. These data were obtained with the main purpose of estimating the cluster fundamental astrophysical parameters. We performed a star count analysis of the cluster fields to assess the clusters' reality as over-densities of stars with respect to the field and estimated the cluster radii. We determined the center of the clusters by finding the maximum surface number density of the stars in each cluster. New equatorial coordinates for the 2000.0 epoch are now provided. We outlined possible solutions for cluster fundamental parameters by matching theoretical isochrones, which reasonably reproduce the main cluster features in the  $(C - T_1, T_1)$  CMDs. In all cases, the best fits were obtained using solar metallicity isochrones. BH 211 was found to be the oldest object of our sample with an age of around 1.0 Gyr. Czernik 37, the most heavily reddened cluster of the sample, with a mean colour excess  $E(B - V) = 1.47$ , is very likely affected by differential reddening. BH 84 is

Table 1: Basic parameters of the four open clusters

Cluster	WEBDA					This study	
	$\alpha_{2000}$ (h m s)	$\delta_{2000}$ ( $^{\circ}$ ' ")	$l$ ( $^{\circ}$ )	$b$ ( $^{\circ}$ )	Diam. (')	$\alpha_{2000}$ (h m s)	$\delta_{2000}$ ( $^{\circ}$ ' ")
BH 84	10 01 19	-58 13 00	280.06	-2.42	4.5	10 01 19	-58 13 33
NGC 5381	14 00 41	-59 35 12	311.60	2.11	11.0	14 00 41	-59 35 20
BH 211	17 02 11	-41 06 00	344.97	0.46	4.0	17 02 10	-41 05 57
Czernik 37	17 53 16	-27 22 00	2.22	-0.64	3.0	17 53 17	-27 22 36

located in the fourth Galactic quadrant just before the tangent to the Carina branch of the Carina-Sagittarius spiral arm. This cluster turned out to be much older than previously believed. Conversely, NGC 5381 was found to be much younger than previously reported. It appears to have a relatively small but conspicuous nucleus and a low-density extended corona. We estimated the angular core and corona radii as  $\sim 2.2'$  and  $\sim 5.7'$ , respectively. The derived fundamental properties for the studied clusters are listed in Table 9. Previous estimates of cluster parameters are listed in Table 10, for easy comparison with the present results. Since two of the studied clusters, BH 211 and Czernik 37, are in the VISTA Variables in the Via Lactea (VVV) survey (Minniti et al., 2010), additional observational information about these two objects can be found in this database.

Table 2: Observation log of observed clusters

Cluster	Date	Filter	Exposure (sec)	Airmass (")
BH 84	May 9, 2008	$C$	30	1.13
		$C$	45	1.13
		$C$	300	1.13
		$C$	450	1.13
		$R$	5	1.13
		$R$	7	1.12
		$R$	30	1.12
		$R$	45	1.12
NGC 5381	May 11, 2008	$C$	90	1.15
		$C$	120	1.15

Table 2 – *continued*

Cluster	Date	Filter	Exposure (sec)	Airmass (")
		<i>C</i>	600	1.15
		<i>C</i>	30	1.16
		<i>R</i>	3	1.16
		<i>R</i>	120	1.16
		<i>R</i>	120	1.16
BH 211		<i>C</i>	30	1.02
		<i>C</i>	45	1.02
		<i>C</i>	300	1.02
		<i>C</i>	450	1.02
		<i>R</i>	5	1.02
		<i>R</i>	7	1.02
		<i>R</i>	30	1.02
		<i>R</i>	45	1.02
Czernik 37	May 10, 2008	<i>C</i>	30	1.00
		<i>C</i>	45	1.00
		<i>C</i>	300	1.00
		<i>C</i>	450	1.00
		<i>R</i>	30	1.00
		<i>R</i>	45	1.00
		<i>R</i>	5	1.00
		<i>R</i>	7	1.00

Table 3: Standard system mean calibration coefficients

<i>C</i>	<i>T</i> <sub>1</sub>
$a_1 = 3.61 \pm 0.03$	$b_1 = 3.04 \pm 0.02$
$a_2 = 0.56 \pm 0.01$	$b_2 = 0.33 \pm 0.02$
$a_3 = -0.19 \pm 0.01$	$b_3 = -0.03 \pm 0.01$



Table 4: CCD  $CT_1$  data of stars in the field of BH 84

Star	$X$ (pixel)	$Y$ (pixel)	$T_1$ (mag)	$\sigma T_1$ (mag)	$C - T_1$ (mag)	$\sigma(C - T_1)$ (mag)	n
495	1870.105	584.378	17.590	0.094	3.237	0.071	1
496	926.421	585.257	15.910	0.018	1.955	0.015	2
497	1568.217	585.395	13.705	0.010	1.653	0.009	1
-	-	-	-	-	-	-	-
-	-	-	-	-	-	-	-

Table 5: CCD  $CT_1$  data of stars in the field of NGC 5381

Star	$X$ (pixel)	$Y$ (pixel)	$T_1$ (mag)	$\sigma T_1$ (mag)	$C - T_1$ (mag)	$\sigma(C - T_1)$ (mag)	n
499	918.737	415.590	13.625	0.005	1.874	0.005	2
500	501.666	418.198	14.553	0.005	1.225	0.005	1
501	1000.223	422.144	16.461	0.022	1.801	0.017	2
-	-	-	-	-	-	-	-
-	-	-	-	-	-	-	-

Table 6: CCD  $CT_1$  data of stars in the field of BH 211

Star	$X$ (pixel)	$Y$ (pixel)	$T_1$ (mag)	$\sigma T_1$ (mag)	$C - T_1$ (mag)	$\sigma(C - T_1)$ (mag)	n
496	1255.054	1053.165	16.858	0.043	2.626	0.034	2
497	1137.926	2039.064	16.899	0.052	2.597	0.040	1
498	983.109	1055.830	15.363	0.016	2.018	0.014	1
-	-	-	-	-	-	-	-
-	-	-	-	-	-	-	-

Table 7: CCD  $CT_1$  data of stars in the field of Czernik 37

Star	$X$ (pixel)	$Y$ (pixel)	$T_1$ (mag)	$\sigma T_1$ (mag)	$C - T_1$ (mag)	$\sigma(C - T_1)$ (mag)	n
500	1480.077	796.860	15.898	0.038	3.126	0.033	1
501	961.983	801.728	15.552	0.021	2.819	0.018	2
502	1114.297	805.020	15.474	0.041	2.794	0.03	1
-	-	-	-	-	-	-	-
-	-	-	-	-	-	-	-

Table 8: Cluster sizes

Cluster	$r_{FWHM}$		$r_{clean}$		$r_{cl}$	
	(px)	(pc)	(px)	(pc)	(pix)	(pc)
BH 84	150	1.0	200	1.3	550	3.6
NGC 5381	150	0.8	280	1.4	1200	6.1
BH 211	150	0.4	250	0.7	580	1.6
Czernick 37	220	0.6	320	0.9	550	1.5

Table 9: Fundamental properties of the observed clusters

Cluster	$E(B - V)$ (mag)	$d$ (kpc)	Age (Myr)	[Fe/H] (dex)	$X$ (kpc)	$Y$ (kpc)	$Z$ (kpc)	$R_{GC}$ (kpc)
BH 84	$0.63 \pm 0.05$	$3.37 \pm 0.48$	$560^{+150}_{-110}$	0.0	7.91	-3.32	-0.14	8.58
NGC 5381	$0.46 \pm 0.04$	$2.63 \pm 0.40$	$250^{+65}_{-50}$	0.0	6.76	-1.97	0.10	7.04
BH 211	$0.61 \pm 0.05$	$1.44 \pm 0.21$	$1000^{+260}_{-200}$	0.0	7.11	-0.37	0.01	7.12
Czernik 37	$1.47 \pm 0.25$	$1.44 \pm 0.86$	$250^{+100}_{-65}$	0.0	7.06	0.06	-0.02	7.06

Table 10: Previous estimates of cluster parameters

Cluster	$E(B - V)$ (mag)	$d$ (kpc)	Age (Myr)	Reference #
BH 84	0.60	$2.92 \pm 0.19$	18	1
NGC 5381	0.06	$1.17 \pm 0.05$	1600	2
BH 211	0.48	$1.38 \pm 0.09$	1600	1
Czernik 37	1.03	$1.73 \pm 0.08$	600	3

References: (1) Bukowiecki et al.(2011); (2) Tadross (2011); (3) Tadross (2008)

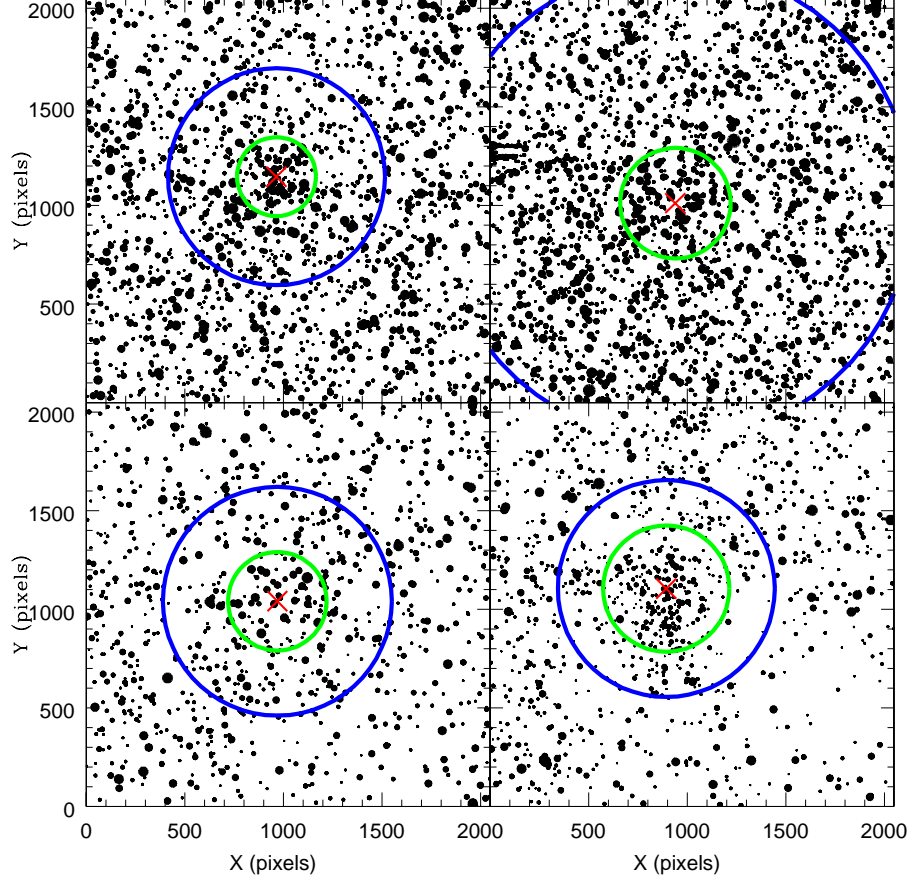


Figure 1: Schematic finding charts of the stars observed in BH 84 (top left), NGC 5381 (top right), BH 211 (bottom left) and Czernik 37 (bottom right). North is up and East is to the left. The sizes of the plotting symbols are proportional to the  $T_1$  brightness of the stars. Two circles  $r_{clean}$  and  $r_{cl}$  wide are shown around the cluster centers (*crosses*).

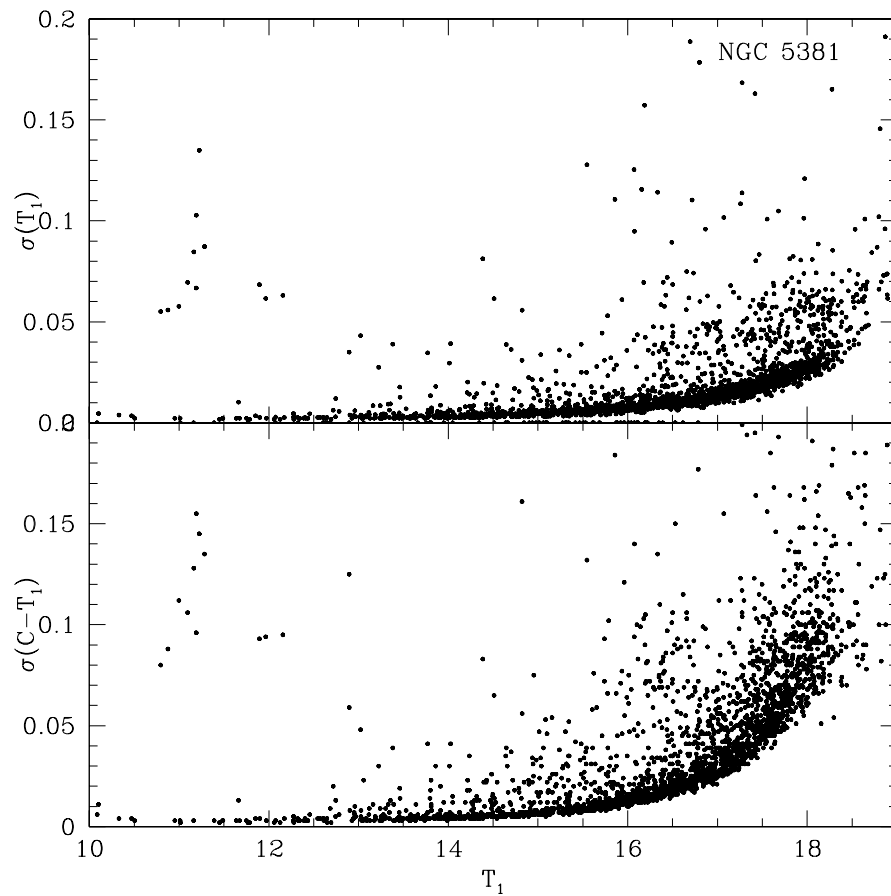


Figure 2:  $T_1$  magnitude and C- $T_1$  color photometric errors as a function of  $T_1$  for stars measured in the field of NGC 5381.

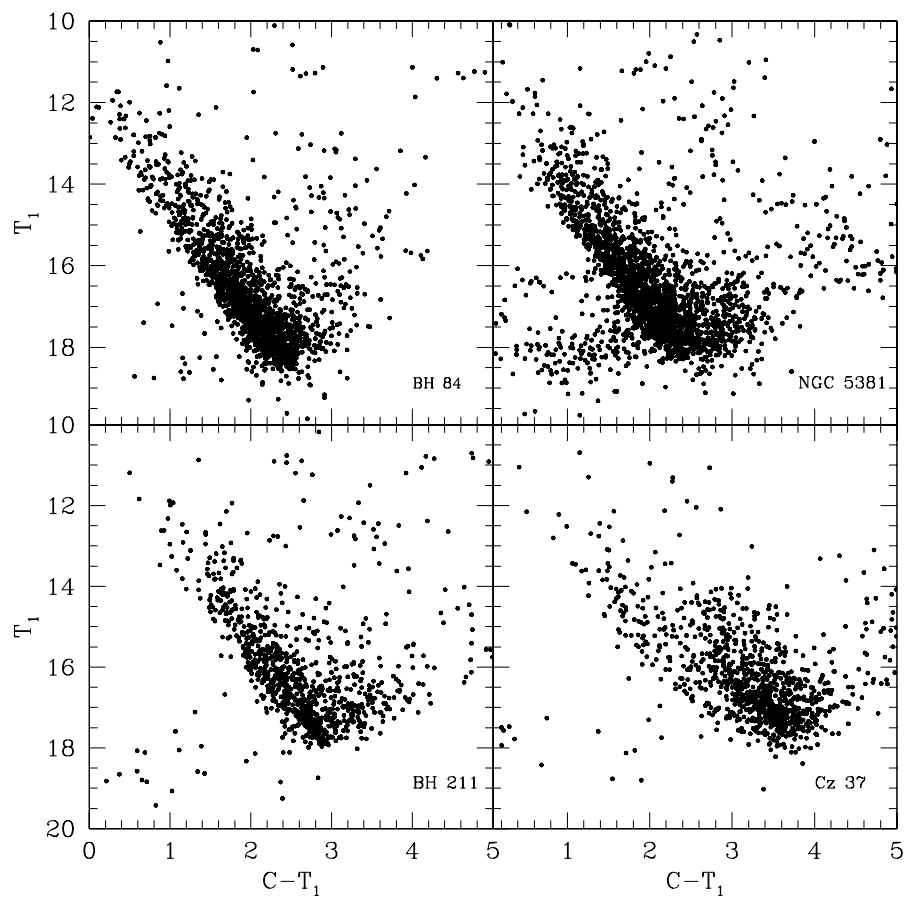


Figure 3:  $(C - T_1, T_1)$  CMDs for stars observed in the field of BH 84, NGC 5381, BH 211 and Czernik 37.

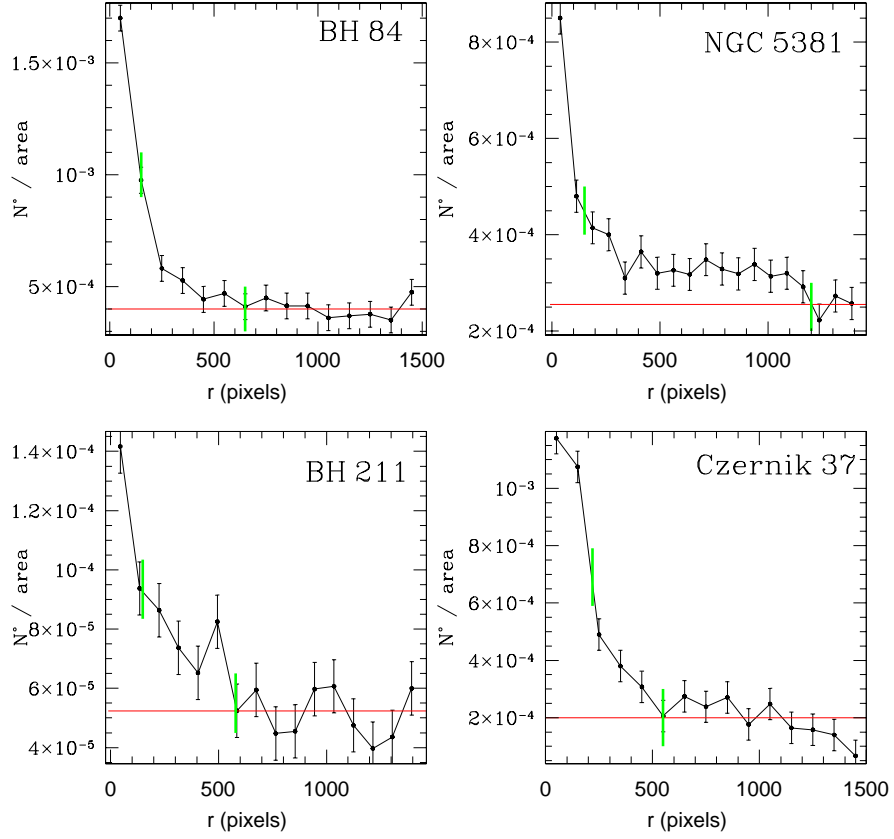


Figure 4: Cluster stellar density radial profiles normalized to a circular area of 50 pixel radius. The radius at the FWHM ( $r_{FWHM}$ ) and the adopted cluster radius ( $r_{cl}$ ) are indicated by green vertical lines. The red horizontal lines represent the measured background levels.

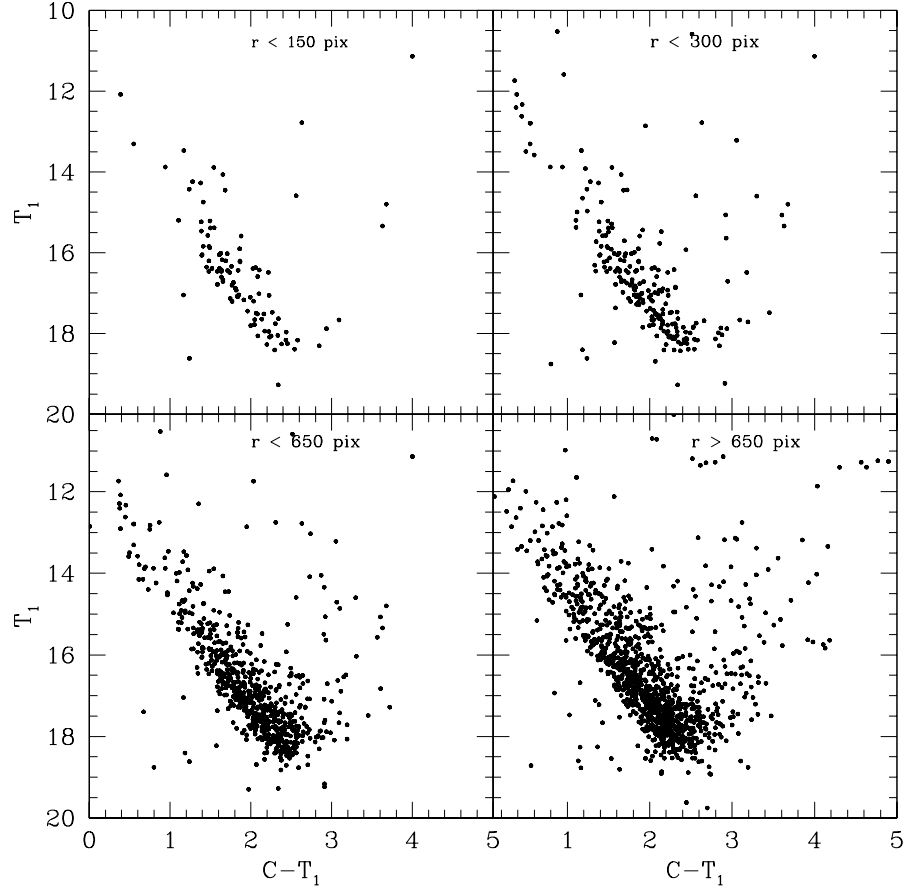


Figure 5: CMDs for stars observed in different extracted circular regions around BH 84 center as indicated in each panel.

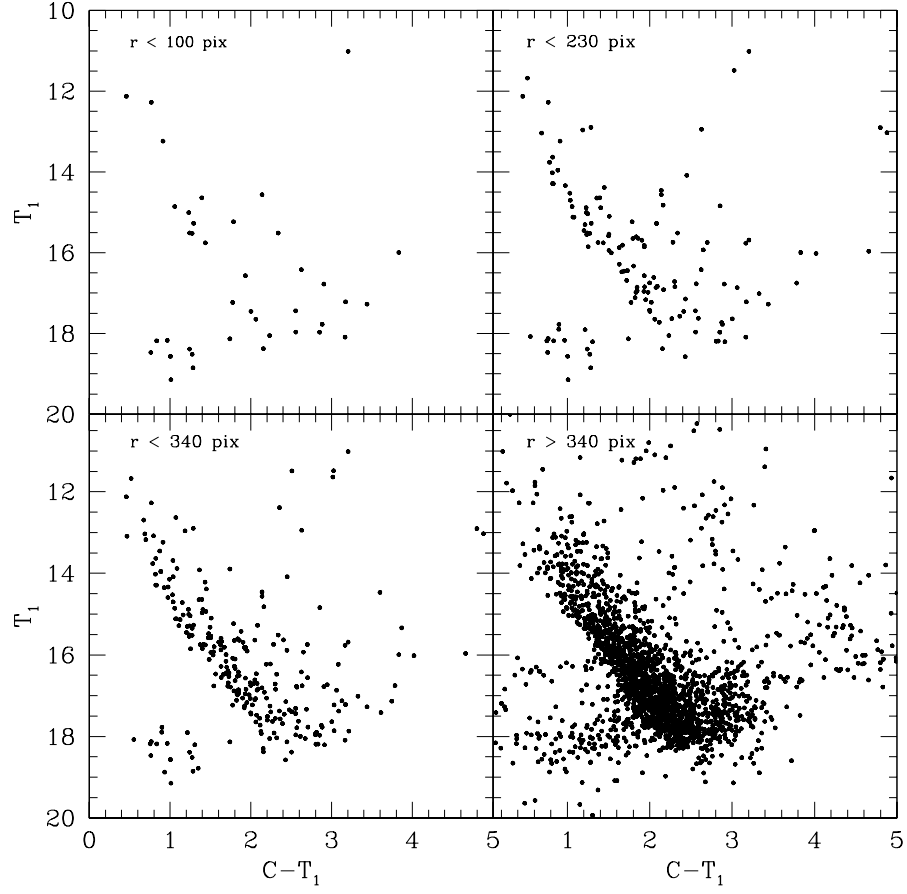


Figure 6: CMDs for stars observed in different extracted circular regions around NGC 5381 center as indicated in each panel.



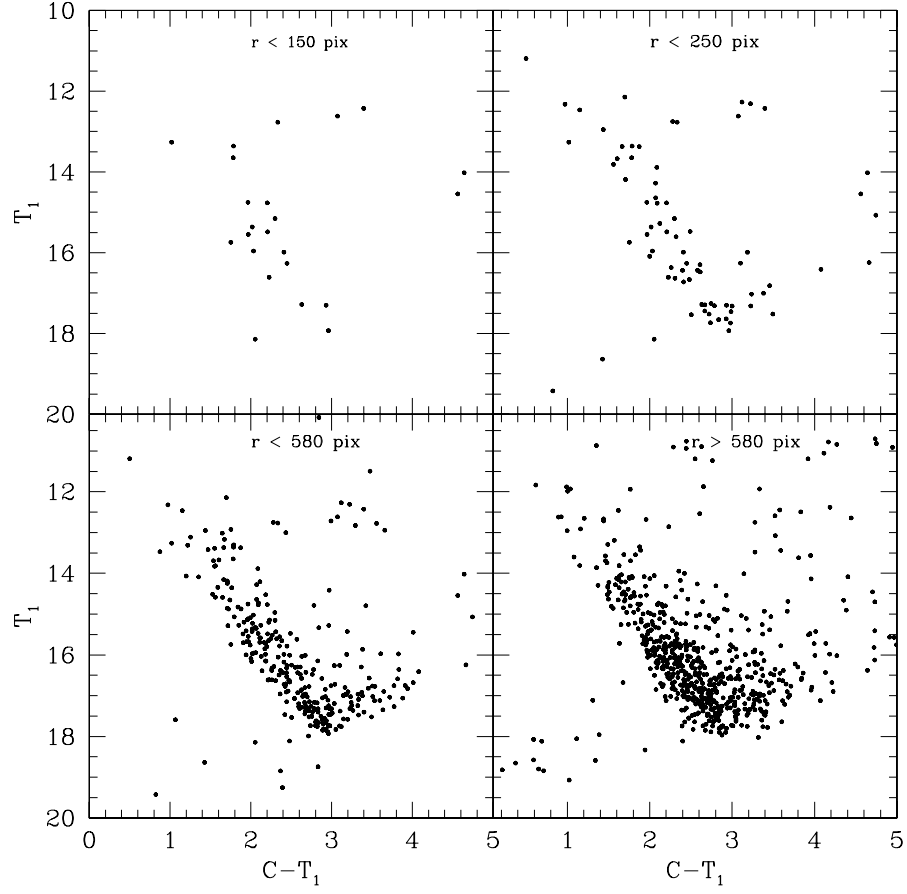


Figure 7: CMDs for stars observed in different extracted circular regions around BH 211 center as indicated in each panel.

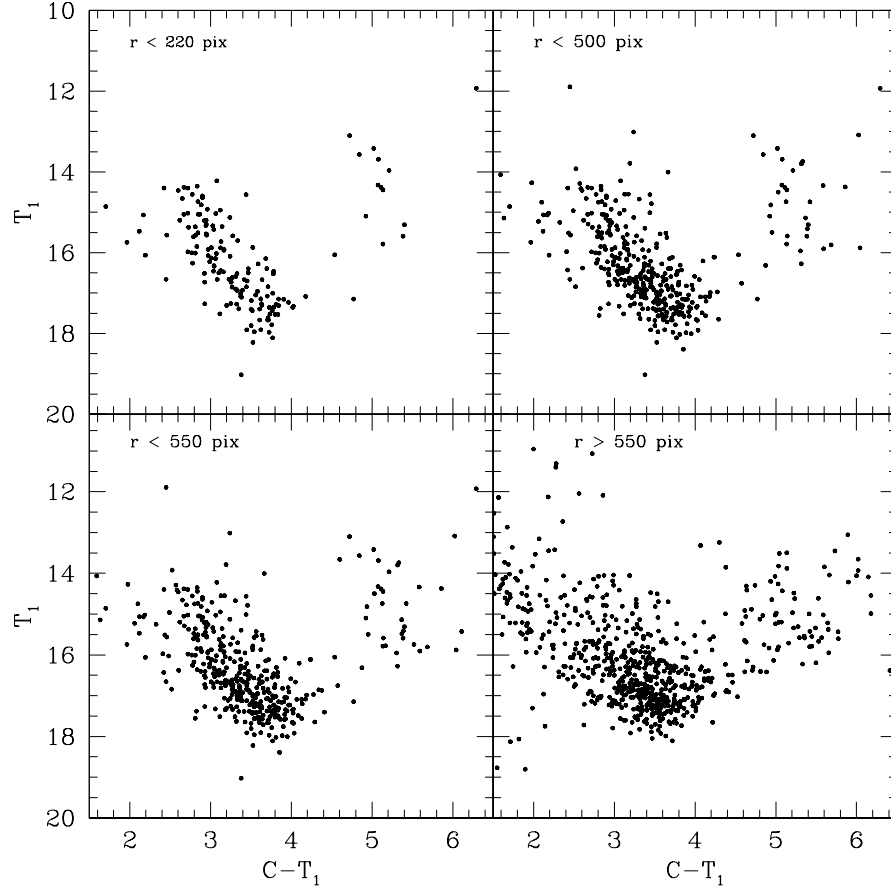


Figure 8: CMDs for stars observed in different extracted circular regions around Czernik 37 center as indicated in each panel.

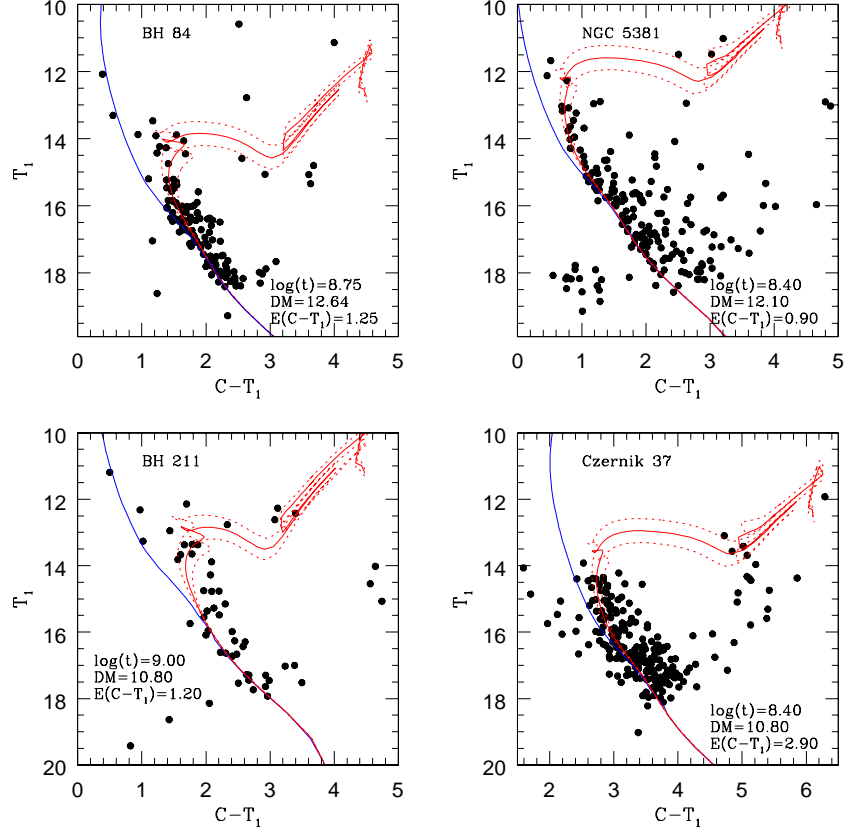


Figure 9:  $r < r_{clean}$   $(C-T_1, T_1)$  CMDs for stars in: BH 84 (top left), NGC 5381 (top right), BH 211 (bottom left) and Czernik 37 (bottom right). The ZAMS and the adopted isochrones from Girardi et al. (2002) are overplotted with solid lines. The isochrones associated to the cluster age errors are indicated by dashed lines, for comparison purposes.

## 7. Acknowledgements

J.J. Clariá, T. Palma and A.V. Ahumada are gratefully indebted to the CTIO staff for their hospitality and support during the observing run. We also thank the anonymous referee for his/her valuable comments and suggestions. This research was partially supported by the Argentinian institutions CONICET, SECYT (Universidad Nacional de Córdoba) and Agencia Nacional de Promoción Científica y Tecnológica (ANPCyT). We have used both the SIMBAD database, operated at CDS, Strasbourg, France, and the NASA's Astrophysics Data System. This work is based on observations made at Cerro Tololo Inter-American Observatory, which is operated by AURA, Inc., under cooperative agreement with the NSF.

## References

- Archinal, B.A., Hynes, S.J., 2003, *Star Clusters*, Willmann-Bell, Inc.
- Bica, E., Bonatto, C., Blumberg, R., 2006, *A&A*, 460, 83
- Bica, E., Dutra, C.M., Soares, J., Barbuy, B., 2003, *A&A*, 404, 223
- Bonatto, C., Bica, E., 2007, *MNRAS*, 377, 1301
- Bonatto, C., Santos Jr., J.F.C., Bica, E., 2006, *A&A*, 445, 567
- Bucokiecki, L., Maciejewski, G., Konoski, P., Strobel, A., 2011, *Acta Astron.*, 61, 231
- Burki, G., 1975, *A&A*, 43, 37
- Canterna, R., 1976, *AJ*, 81, 228
- Carraro, G., Janes, K.A., Eastman, J.D., 2005, *MNRAS*, 364, 179
- Clariá, J.J., Piatti, A.E., Parisi, M.C., Ahumada, A.V., 2007, *MNRAS*, 379, 159
- Chen, L., Hou, J.L., Wang, J.J., 2003, *AJ*, 125, 1397
- Czernik, M., 1966, *Acta Astron.*, 16, 93
- Dias, W.S., Alessi, B.S., Moitinho, A., Lépine, J.R., 2002, *A&A*, 389, 871

- Dias, W.S., Monteiro, H., Caetano, T.C., Oliveira, A.F., 2012, A&A, 539, 125
- Dutra, C.M., Bica, E., Soares, J., Barbuy, B., 2003, A&A, 400, 533
- Friel, E.D., 1995, ARA&A, 33, 38
- Geisler, D., 1996, AJ, 111, 480
- Geisler, D., Sarajedini, A., 1999, AJ, 117, 308
- Girardi, L., Bertelli, G., Bressan, A., Chiosi, C., Groenewegen, M.A.T. et al., 2002, A&A, 391, 195
- Kronberger, M., Teutsch, P., Alessi, B. et al., 2006, A&A, 447, 921
- Lejeune, T., Schaerer, D., 2001, A&A, 366, 538
- Lyngå, G., 1982, A&A, 109, 213
- Marcionnni, N., Parisi, M.C., Clariá, J.J., Ahumada, A.V. et al., 2013, ASP Conference Series (in press).
- Mermilliod, J.-C., 2005, WEBDA Open Cluster Database, <http://obswww.unige.ch/webda/>
- Minniti, D., Lucas, P., Emerson, J.V. et al., 2010, New Astron., 15, 433
- Parisi, M.C., Clariá, J.J., Piatti, A.E., Geisler, D., 2005, MNRAS, 363, 1247
- Piatti, A.E., Bica, E., Geisler, D., Clariá, J.J., 2003b, MNRAS, 344, 965
- Piatti, A.E., Clariá, J.J., Ahumada, A.V., 2003a, MNRAS, 340, 1249
- Piatti, A.E., Clariá, J.J., Ahumada, A.V., 2004, A&A, 418, 979
- Pietrzyński, G., Kubiak, M., Udalski, A., Szymański, M., 1997, Acta Astron., 14, 97
- Piskunov, A.E., Kharchenko, N.V., Roser, S., Schilbach, E., Scholz, R.D., 2006, A&A, 445, 545
- Portegies Zwart, S.F., McMillan, S.L.W., Gieles, M., 2010, ARA&A, 48, 431

- Soares, J.B., Bica, E., 2002, *A&A*, 388, 172
- Stetson, P.B., 1991, DAOPHOT User Manual (Victoria, B.C: Dominion Astrophys. Obs., Herzberg Inst. Astrophys.
- Stetson, P.B., 1994, *PASP*, 106, 250
- Tadross, A.L., 2008, *New Astron.*, 13, 370
- Tadross, A.L., 2011, *J. Korean Astron., Soc.*, 44, 1
- van den Bergh, S., Hagen, G.L., 1975, *AJ*, 80, 11